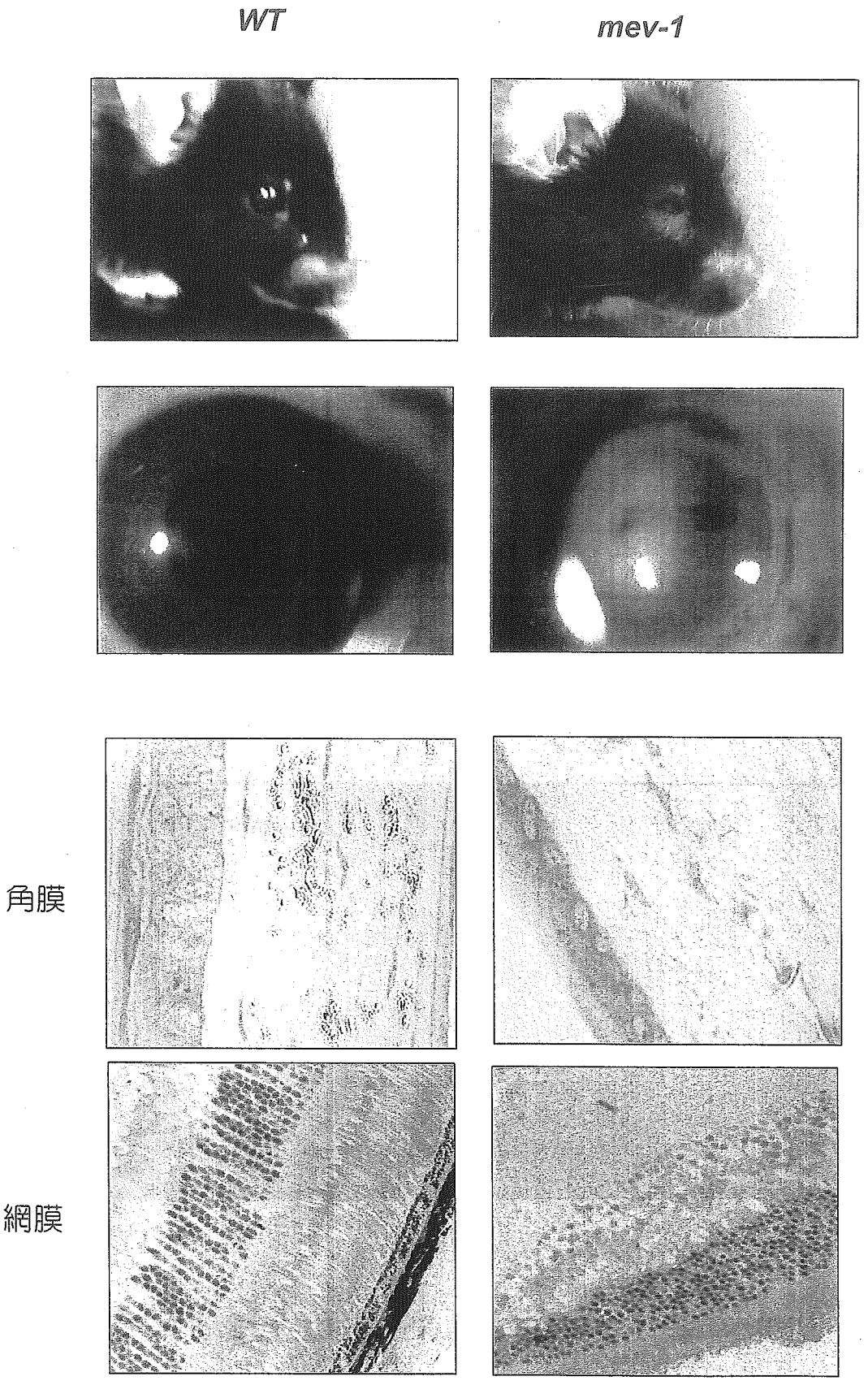

図8　角膜および網膜異常

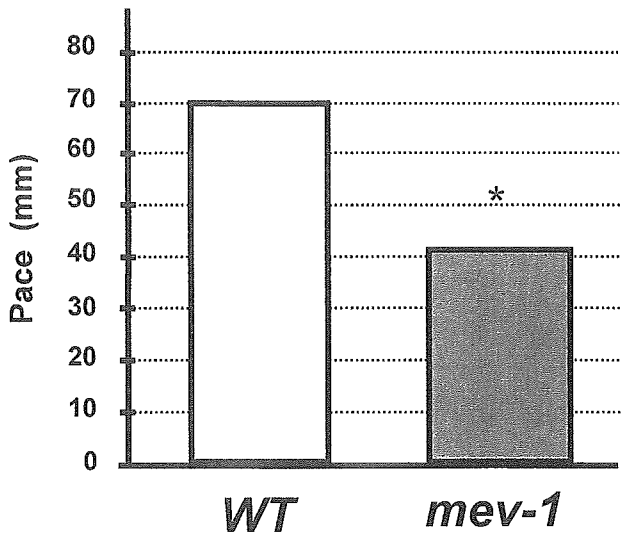

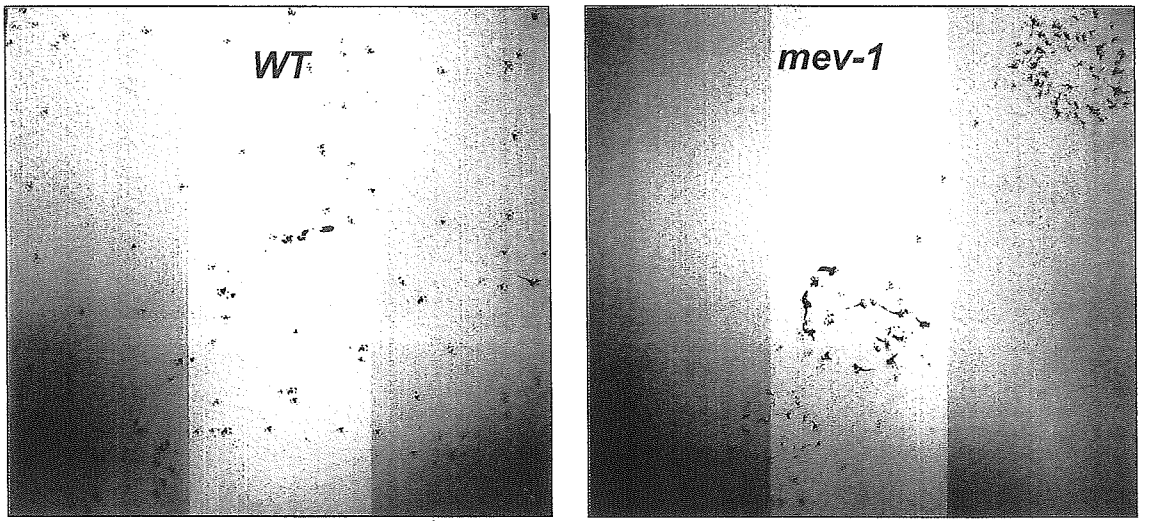

図9　直線歩行幅、オープンフィールドテストから確認される運動能力
上図　直線歩行幅;　下図　オープンフィールドテスト

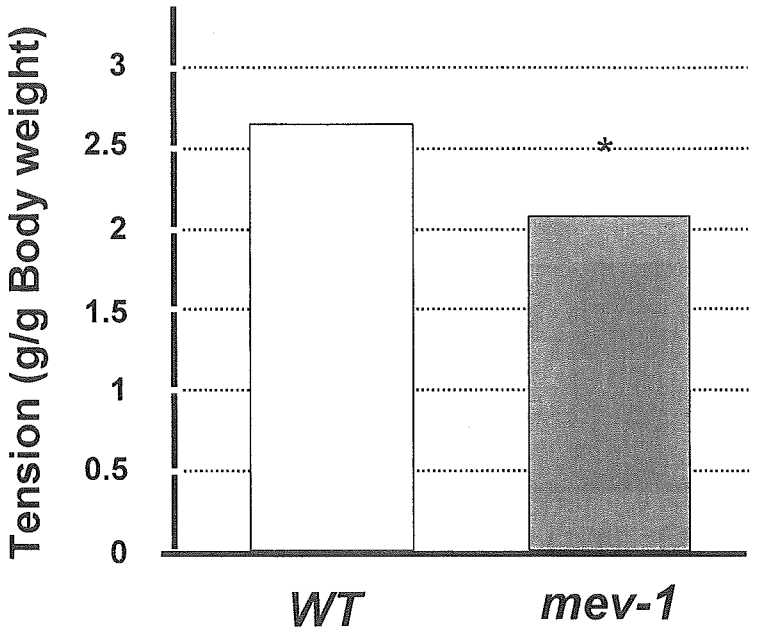

図10　筋肉繊維張力の低下

	WT	*mev-1*
	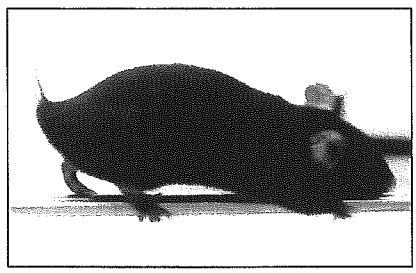	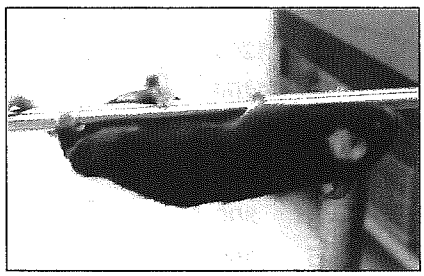
20cm-6mm pipe	**10.3±2.2 (sec./20cm-6mm pipe)**	**42.0±16.0 (sec./20cm-6mm pipe) Stationary state: 4 times Falling: 1 time**
20cm-3mm pipe	**11.2±3.2 (sec./20cm-3mm pipe)**	**73.0±28.3 (sec./20cm-3mm pipe) Stationary state: 3 times Falling: 3 times**

図11　運動能力

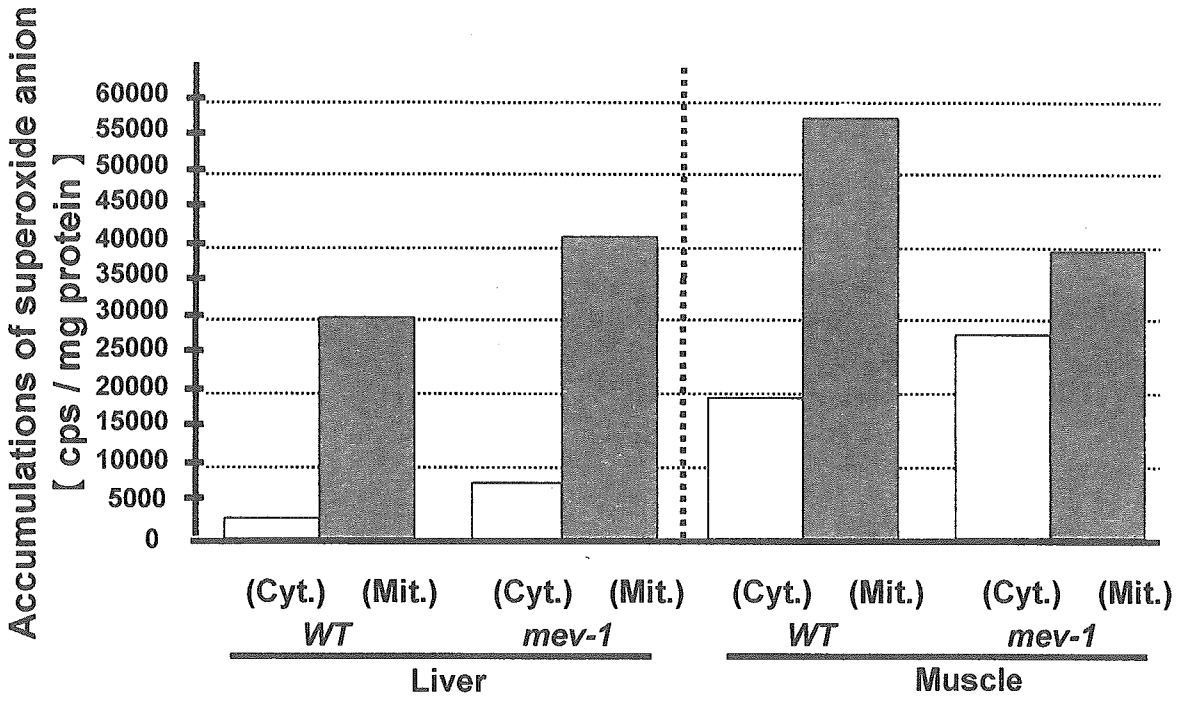

図12　細胞内活性酸素蓄積量

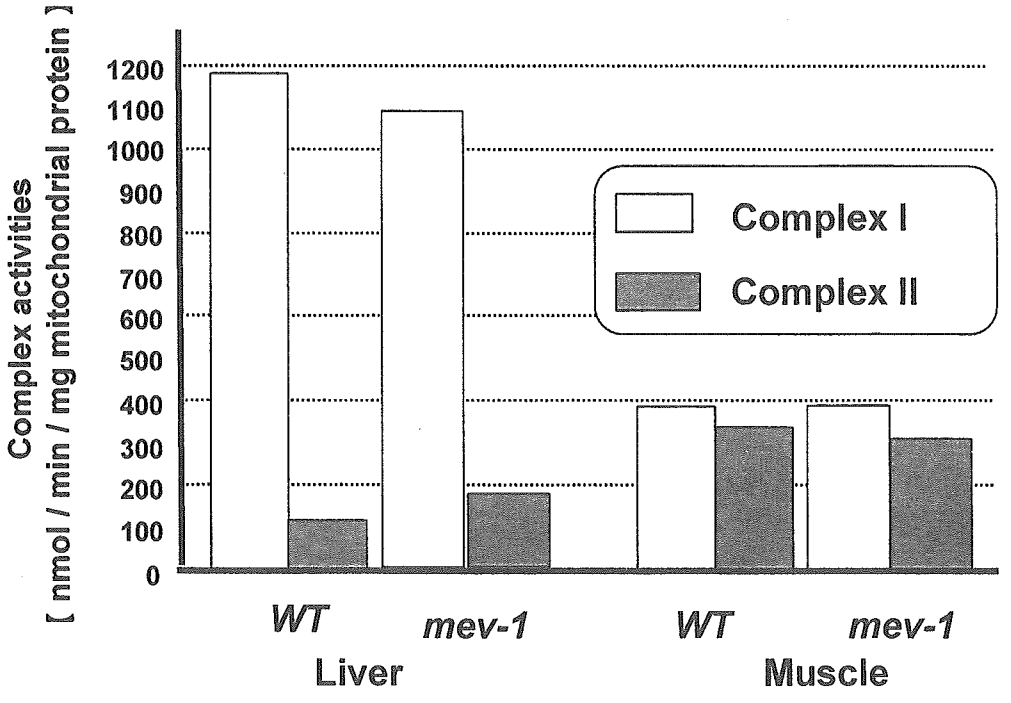

図13　ミトコンドリア電子伝達系酵素活性

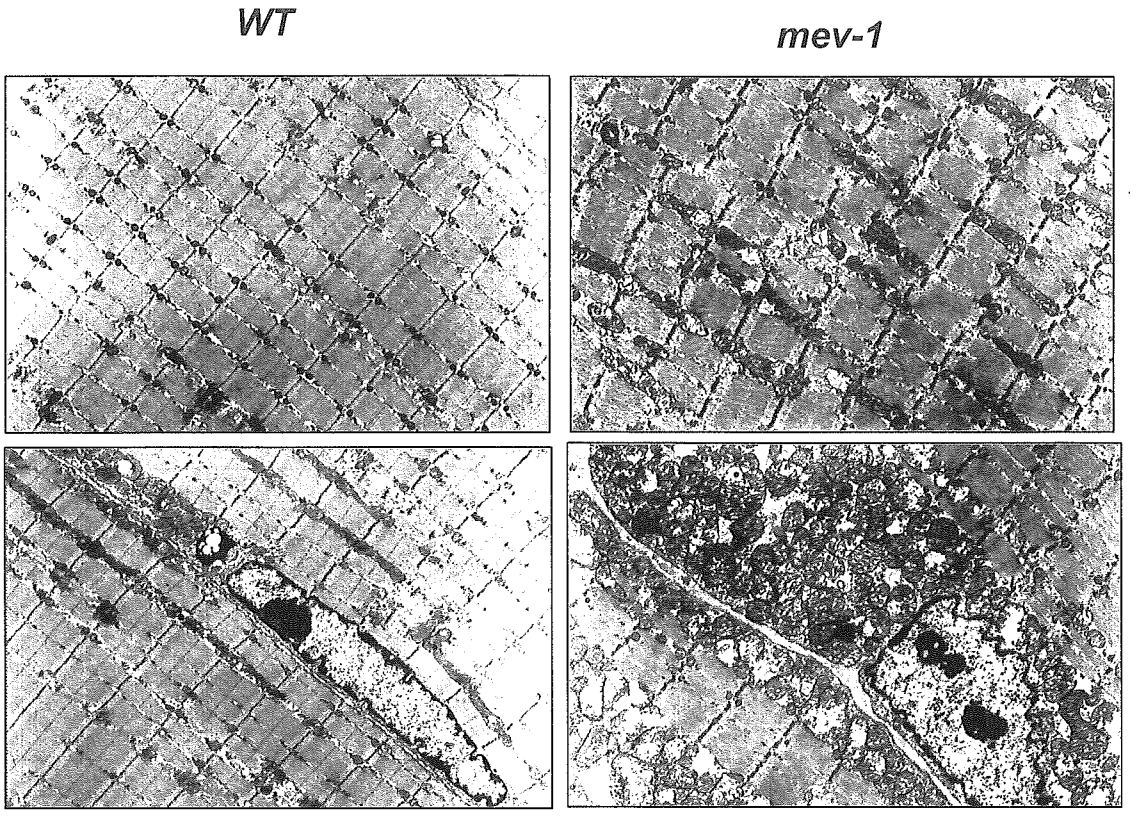

図14　筋繊維細胞内のミトコンドリアの構造異常と筋繊維の破壊

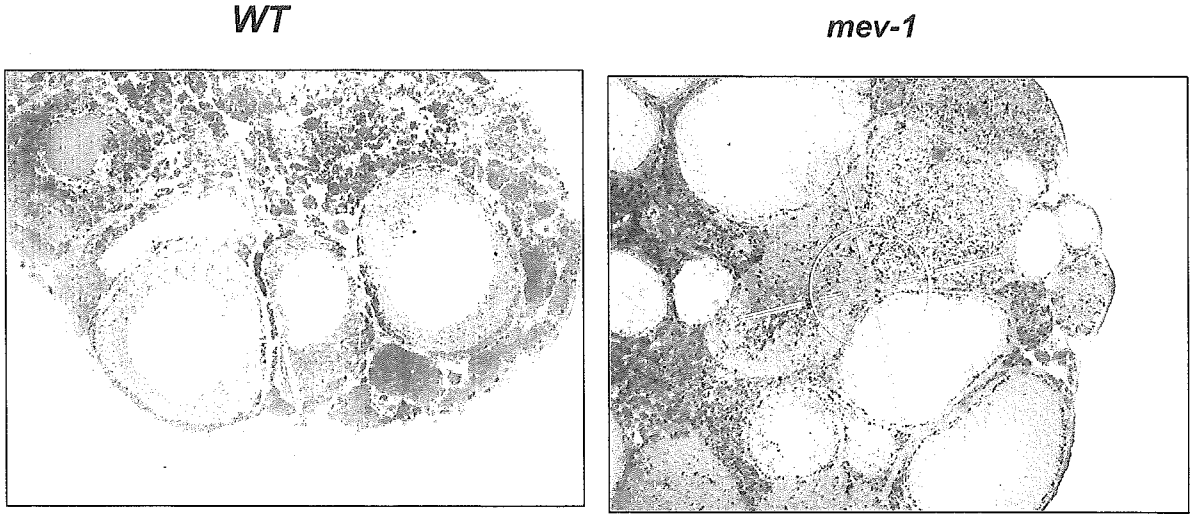

図15　生殖器官　（卵子の成熟）

研究成果の刊行に関する一覧表

雑誌

発表者氏名	論文タイトル	発表誌名	巻号	ページ	出版年
Suda H Shouyama T Yasuda K Ishii N	Direct measurement of oxygen consumption rate on the nematode *Caenorhabditis elegans* by using an optical technique	Biochem. Biophys. Res. Comm.	330	839-843	2005
Kondo M Senoo-Matsuda N, Yanase S Ishii N Hartman PS Ishii N	Effect of oxidative stress on translocation of DAF-16 in oxygen-sensitive mutants, *mev-1* and *gas-1* of *Caenorhabditis elegans*	Mech. Ageing Develop.	126	637-641	2005
Kondo M Yanase S Ishii T Hartman PS Matsumoto K Ishii N	The *p38* signal transduction pathway participates in the oxidative stress-mediated translocation of DAF-16 to *Caenorhabditis elegans* nuclei	Mech. Ageing Develop.	126	642-647	2005

研究成果の刊行物

Available online at www.sciencedirect.com
SCIENCE DIRECT®
ELSEVIER
Biochemical and Biophysical Research Communications 330 (2005) 839–843
BBRC
www.elsevier.com/locate/ybbrc

Direct measurement of oxygen consumption rate on the nematode *Caenorhabditis elegans* by using an optical technique

Hitoshi Suda [a,*], Tetsuji Shouyama [a], Kayo Yasuda [b], Naoaki Ishii [b]

[a] *Department of Biological Science and Technology, School of High-Technology for Human Welfare, Tokai University, 317 Nishino, Numazu, Shizuoka 410-0321, Japan*
[b] *Department of Molecular Life Science, School of Medicine, Tokai University, Bohseidai, Isehara, Kanagawa 259-1193, Japan*

Received 21 February 2005
Available online 17 March 2005

Abstract

It is well known that aging and longevity strongly correlate with energy metabolism. The nematode *Caenorhabditis elegans* is widely used as an ultimate model of experimental animals. Thus, we developed a novel tool, which is constructed from an optical detector, using an indirect method that can measure simply the energy metabolism of *C. elegans*. If we measure the oxygen consumption rate using this optical tool, we can easily evaluate the activity of mitochondria as an index in the aging process. However, a direct measurement of the oxygen consumption rate of *C. elegans* exposed in air is thought to be impossible because of the high concentration of atmospheric oxygen and the small size of the animals. We demonstrate here that we can directly detect the oxygen consumption with a small number of animals ($\leqslant$40) and a short accumulation time ($\leqslant$30 min) at high precision by using both an optical probe and a small chamber. The metabolic rate of a 4-day-old hermaphrodite animal, for example, was approximately 80 nW. Our method using *C. elegans* has the potential to become a useful technique for research on aging correlated with energy metabolism.

Keywords: Ageing; Life span; *Caenorhabditis elegans*; Metabolism; Oxygen consumption

In order to elevate the quality of life, one of the scientific missions of this century is to understand the aging process at a molecular level. Recent research has made it well known that aging and longevity strongly correlate with energy metabolism based on the following lines of evidence: (i) the insulin/insulin-like growth factor I (IGF-I) pathway of signal transduction is related to aging [1], (ii) caloric restriction is related to the extension of longevity [2], and (iii) aging is closely related to the function of mitochondria [3]. The nematode *Caenorhabditis elegans* is a very useful animal to use in investigating the molecular basis of aging because its genetic information has been established and its maximum life span is very closely related to energy metabolism. Thus, it is important to quantitatively evaluate the activity of mitochondria on *C. elegans*. In this work, we developed a novel tool to measure directly the oxygen consumption rate in a whole body on *C. elegans*. The activity of isolated mitochondria or each complex is often measured in vitro, but in this study we carried out the measurement on a whole body because we wanted to know how the respiratory activity of the whole body changes with aging. The tool we developed is very simple and is a convenient way to study the aging process on *C. elegans*.

Recently, Vanfleteren and co-workers [4–6] systematically investigated the energy metabolic rate of *C. elegans* in liquid medium by using direct and indirect methods employing a micro-calorimeter and a Clark-type electrode, respectively. They used about 8000 animals per measurement and required 30 min per

* Corresponding author. Fax: +81 55 968 1156.
E-mail address: suda@fb.u-tokai.ac.jp (H. Suda).

0006-291X/$ - see front matter © 2005 Elsevier Inc. All rights reserved.
doi:10.1016/j.bbrc.2005.03.050

measurement. On the other hand, Van Voorhies and Ward [7] indirectly determined the metabolic rate of *C. elegans* exposed in air by using a mass spectrum to measure the produced concentration of carbon dioxide (CO_2). They also used about 50 animals per measurement and spent 5–6 h per measurement to detect the effective signal. We tried the direct measurement of oxygen concentration to determine respiratory activity. The direct measurement of the oxygen consumption rate of *C. elegans* exposed in air has been thought to be impossible because of the high concentration of atmospheric oxygen. However, we succeeded in overcoming this difficulty by using a chamber of small volume. In our experimental system, we used 1–40 animals, and the time required for one measurement was 20–30 min. These points are merits of our method.

Materials and methods

Culture of nematode C. elegans and preparations of measurements. In this study, we used wild-type (N2) hermaphrodite animals. The animals were cultured on nematode growth medium (NGM) and *Escherichia coli* OP50, a uracil-requiring mutant. NGM was concretely made as follows. Seven grams of agar (Difco), 3 g of NaCl, and 1.5 g of peptone (Difco) were added to 975 ml distilled water. The medium was autoclaved, cooled to 60 °C, and supplemented with 1 ml cholesterol (5 mg/ml in 99.5% ethanol), 1 ml of 1 M $CaCl_2$, 1 ml of 1 M $MgSO_4$, and 25 ml of 1 M KH_2PO_4 buffer (pH 6.0). The solution was poured into large (92 mmΦ × 15 mm) or small (35 mmΦ × 10 mm) Petri dishes. The bacteria were grown on autoclaved LB liquid (10 g tryptone (Difco), 5 g yeast extract (Difco), and 10 g NaCl in 1 liter distilled water) at 37 °C overnight. The bacteria were spread onto the surface of NGM agar plates and grown to a confluent lawn at highly controlled room temperature, 22 ± 1 °C.

Synchronized animals were used to measure oxygen consumption and life spans. Animals were synchronized by culturing eggs in an S-buffer (0.1 M NaCl, 0.05 M potassium phosphate buffer (pH 6.0)) at 20 °C for 1 day. The eggs were isolated from 4-day-old adults at 20 °C, as previously described [8–10]. The age (x) denotes the time after hatching (0 = time of hatching). Survivorship was determined using animals cultured in small Petri dishes [8,11]. We used 10 animals per dish and 100 animals per measurement. Death was determined to have occurred when the animal ceased to move. To get a precise count of survivors, progeny produced from parents on the small Petri dishes were removed. This was achieved using a picker made from thin platinum wire, a special tool that is usually used to transfer *C. elegans* from one dish to another. We measured survivorship at 25 °C. After this measurement, the dead animals were removed from the Petri dish with a picker.

To measure the metabolism, the animals were classified according to age as follows. To remove progeny from large dishes, instead of using a picker, we separated adults and larvae several times with reference of the difference in their sedimentation rate in a conical tube (15 ml) filled with a 10 ml S-buffer. Each separation was carefully carried out within 10 min in order to prevent great damage to the animals. We verified that this procedure had a negligible effect on respiratory activity.

Measurement of oxygen consumption. The metabolic rate of animals was determined using an indirect method as the oxygen consumption rate. Oxygen concentration was measured using an optical oxygen sensor, a spectrometer-coupled chemical sensor for full spectral analysis of dissolved or gaseous oxygen pressure (FOXY-2000, Ocean Photonics, Japan). The conceptual diagram of the experiment is shown in Fig. 1A. The fluorescence method measures the partial pressure of dissolved or gaseous oxygen. An optical fiber carries excitation light (475 nm) produced by a blue LED to a thin film coated by a ruthenium complex at the probe tip. The probe collects fluorescence (600 nm) generated at the tip and carries it via another optical fiber to the high-sensitivity spectrometer. Here, we used a 300-μm aluminum-jacketed fiber-optic probe. When oxygen in the gas or liquid sample diffuses into the thin film coating, it quenches the fluorescence. The degree of quenching correlates to the level of partial pressure of oxygen. The fluorescence is related quantitatively to the partial pressure of oxygen in terms of the Stern–Volmer equation; $I_0/I = 1 + kp_{O_2}$, where I_0, I,

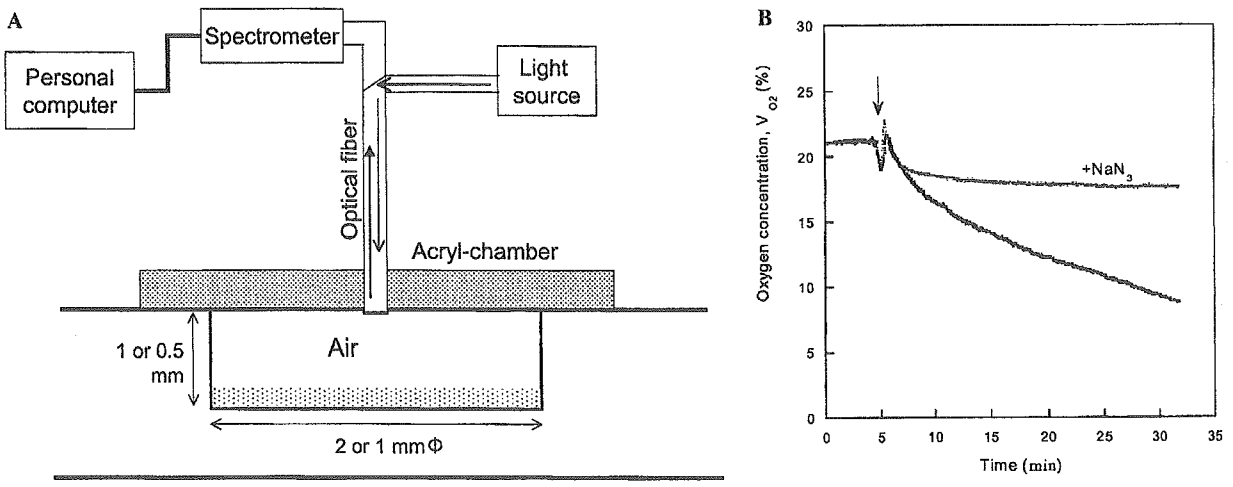

Fig. 1. (A) Block diagram of the direct measurement of the oxygen consumption for the system of *C. elegans*. See the text for details regarding the method. (B) Typical data of the oxygen consumption using wild-type strain. The number of animals transferred from a large Petri dish to a standard chamber, which were cultured for 4 days at 20 °C, was 40. A control experiment was performed by adding to the animal-immersed medium a 0.5-μl solution of sodium azide (NaN_3, 10 mM), which inhibits the cytochrome oxidase in the oxidative phosphorylation and gradually stops the respiratory chain. Recording of data was started about 10 min after the addition of sodium azide. Note that both time courses were adjusted at the sealing position, which is marked with an arrow.

and k represent the intensity of fluorescence at zero pressure of oxygen, the intensity of fluorescence at pressure p_{O_2} of oxygen, and the Stern–Volmer constant, respectively. For a given medium and at a constant total pressure and temperature, the partial pressure of oxygen is proportional to the oxygen concentration. The linear Stern–Volmer algorithm requires two standards of known oxygen concentration. The zero calibration of oxygen concentration V_{O_2} was adjusted with sodium sulfite (1.5 g per 50 ml of super-purified water (Milli-Q Labo, Millipore)), which perfectly deoxidized the solution. This zero-position was quite equal to the level in 100% nitrogen gas. Another standard was calibrated with air ($V_{O_2} = 20.9\%$).

The oxygen consumption rate on *C. elegans* was measured on 1–40 animals in a closed chamber with a volume of 0.4 μl (0.5 mm thickness × 1 mmΦ diameter; small chamber) or 3.1 μl (1 mm × 2 mmΦ; standard chamber). Using a picker, animals were transferred from a Petri dish into one of the chambers, which was immersed in 0.1 μl (for the small chamber) or 0.4 μl (for the standard chamber) of a liquid medium with the same composition as that of NGM, except for agar, including bacteria ($>3 \times 10^8$ cells/ml). After the transfer, the chamber was immediately sealed with silicon grease (Shin-Etsu Chemical, Japan). Each oxygen measurement was carried out within about 30 min at 22 ± 1 °C. The energy metabolic rate of each animal (W) was approximately converted from the oxygen consumption rate of each animal using an energy equivalent of 20.1 J per 1 ml of oxygen [7]. We measured the cross-section (of long direction) of animals as an index of size using the Scion image software (Scion, USA).

Results and discussion

As illustrated in Fig. 1A, to measure the oxygen consumption, the animals were transferred from the large Petri dishes and immersed in a small amount of liquid medium in a sample chamber of small volume. The liquid medium was employed to keep the animals in the chamber alive. Indeed, they could survive in this medium for at least 12 h provided the evaporation of water was completely prevented. Fig. 1B shows typical data of the direct measurement of the oxygen consumption by

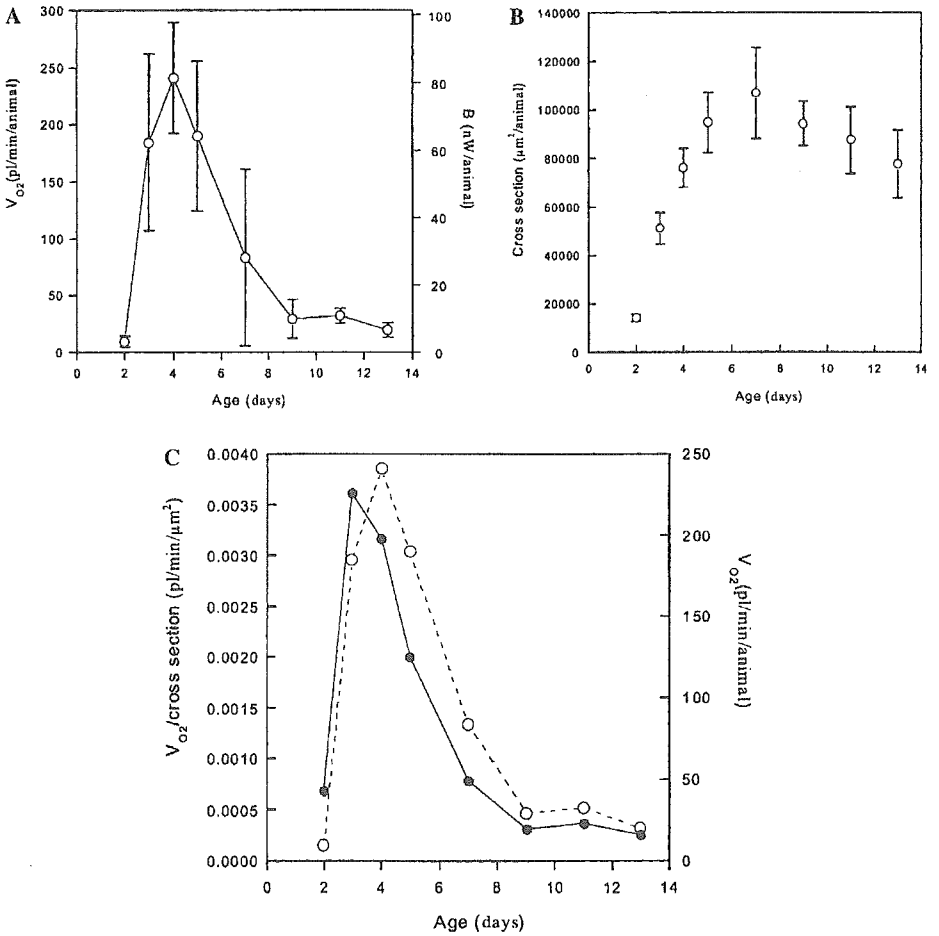

Fig. 2. (A) Oxygen consumption rate per animal $\dot{V}_{O_2}$ (pl/min/animal) as a function of age. Using a standard chamber, we measured the oxygen consumption rates on 20 animals that were cultured at 25 °C. The right axis represents the converted energy metabolism per animal, B (nW/animal). Each data point is the mean value of three different measurements, where error bars represent the standard deviation. (B) Cross-section of animals as a function of age in units of μm². The average was taken for about 20 animals. Error bars are the standard deviation. (C) Oxygen consumption rate per cross-section $\dot{V}_{O_2}$ (pl/min/μm²). These data were calculated by dividing (A) by (B). Open and filled circles are $\dot{V}_{O_2}$ per animal and per unit cross-section, respectively.

the wild-type strain at 20 °C. As soon as the chamber was tightly sealed with silicon grease, the signal quickly changed in an up-and-down manner, as shown by the arrow in Fig. 1B, because of the influence of sealing. After this temporary change, the signal decreased gradually. A linear region could be usually observed after about 5 min. From the slope of this straight line, we calculated the oxygen consumption $\dot{V}_{O_2}$ of all the animals, which was 0.301% per min in this case. For 40 animals (4-day-old animals after hatching) in a chamber volume of 3.1 μl, the oxygen consumption per animal obtained was 236 pl/min/animal. This oxygen consumption was converted to a metabolic rate of 79.1 nW/animal by the use of the energy equivalent, 20.1 J/ml oxygen [7]. This metabolic rate is fairly consistent with that of Van Voorhies and Ward [7]. To check whether our detected signal was truly due to the respiratory of the animals, we added a solution of sodium azide to the standard chamber at the end of this measurement process. Sodium azide is a harmful reagent that specifically inhibits respiration. The chamber was sealed after about 10 min from the addition. In Fig. 1B, it is shown that the respiratory rate was significantly depressed, as expected. From this control experiment, our method was verified as capable of accurately detecting the rate of oxygen consumption of *C. elegans*. Although we did not measure the oxygen consumption rate on animals exposed to air, we obtained a good result, probably because of the very rapid exchange of oxygen molecules between a small amount of liquid medium and a gas or air phase. Since the amount of liquid in each chamber was very small, the concentration of oxygen around each animal might have become uniform quickly. The uniformity of oxygen in a liquid surrounding an animal could be established in an instant in the small space by the diffusion of oxygen molecules and the twisting motion of animals. Thus, our experimental condition appears to be nearly equal to that of animals exposed in air.

The oxygen consumption per animal $\dot{V}_{O_2}$ (pl/min/animal) is plotted as a function of age in Fig. 2A. On the other hand, Vanfleteren et al. [4–6] pointed out that $\dot{V}_{O_2}$ should be expressed by $\dot{V}_{O_2}$ per volume or protein weight. The quantity $\dot{V}_{O_2}$ per volume seems to symbolize the activity of each cell or mitochondrion. Therefore, the behavior of $\dot{V}_{O_2}$ per animal in terms of aging is essential in comparison with that of the survival curve because both sets of data have to be closely related to the individuals rather than to each cell.

Let us compare our result with that of Vanfleteren et al. to verify the accuracy of our method. Fig. 2B shows the cross-section (of long direction) of animals that were used in the experiment shown in Fig. 2A. Usually, a volume is proportional to the cross-section raised to the 1.5th power. The cross-section of *C. elegans* from larva to adult highly correlated with the volume of *C. elegans* because of the geometric similarity of the body formation. The relationship between volume and cross-section was given by volume (nl) $= 1.849 \times 10^{-7}$ (nl/μm^3) $\times$ area$^{1.5}$ (μm^3) and correlation coefficient $= 0.9974$ (personal communication with Fujiwara [12]). However, a linear approximation may be conveniently supposed in a narrow region of 1–5.5 nl as volume (nl) $= -1.202 + 6.678 \times 10^{-5} \times$ area (μm^2) and correlation coefficient $= 0.9954$. Thus, $\dot{V}_{O_2}$ per cross-section may be approximately interpreted to equal $\dot{V}_{O_2}$ per volume. As shown in Fig. 2C, both cases are superimposed for comparison. The behavior of the time course of $\dot{V}_{O_2}$ per cross-section is in good agreement with that of $\dot{V}_{O_2}$ per protein weight as measured by Vanfleteren et al. As they pointed out, the peak of

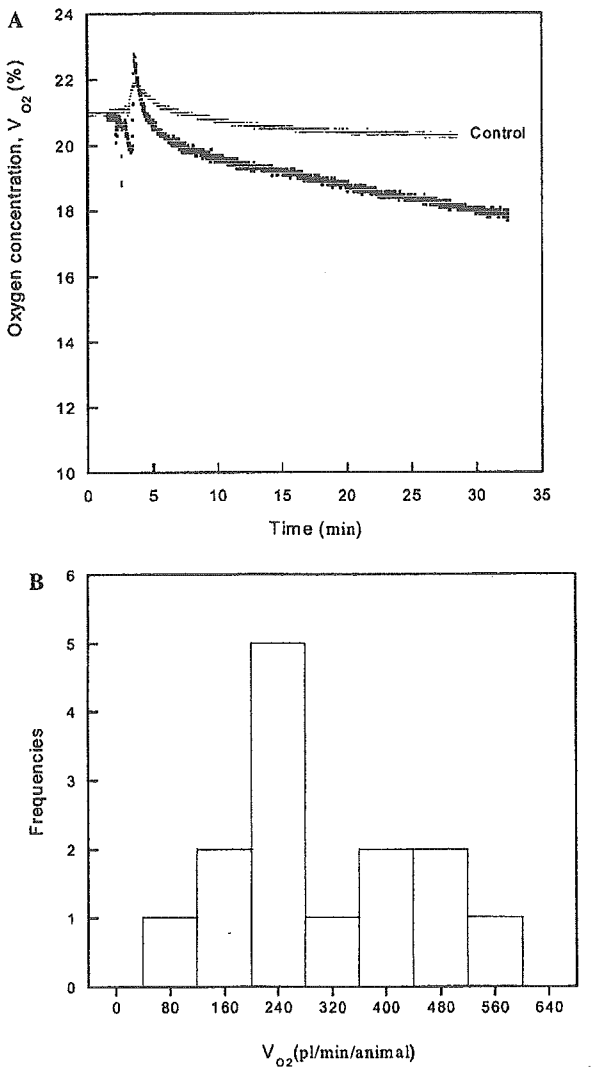

Fig. 3. The oxygen consumption rate $\dot{V}_{O_2}$ per single animal. The oxygen consumption rate was measured using a small chamber on a single animal that was cultured at 20 °C for 4 days after hatching. (A) Typical data of a single animal. The $\dot{V}_{O_2}$ of the single animal was 363 pl/min. The thin dots represent the data in the absence of an animal as a control experiment. (B) Histogram of $\dot{V}_{O_2}$ The number of different measurements was 14.

$\dot{V}_{O_2}$ (pl/min/μm^2) was similarly revealed at the larval stage, and after the peak it decreased sharply. On the other hand, the peak in $\dot{V}_{O_2}$ (pl/min/animal) was exhibited on 4-day-old adults, while the peak of reproduction usually came on the fourth or fifth day [13] and then decreased exponentially. The coincidence of these two peaks is a plausible result because a great deal of energy would be needed to produce a large number of eggs or the potential.

If we use a small chamber, we can measure the oxygen consumption on a single animal, as shown in Fig. 3. Because we usually used the standard chamber and 20 or 40 animals, we measured the average oxygen consumption rate of all the animals. We saw that there was a large standard deviation, as shown in Fig. 2A. By measuring the $\dot{V}_{O_2}$ of a single animal, we determined the potential ability of a single animal. Fig. 3A indicates the stability of a signal in the single system. In fact, we found that the metabolic rates of individual animals varied widely and the maximum potential exceeded 500 pl/min, as shown in Fig. 3B. Perhaps, this large dispersion is a reason for the sigmoid formation in the survival curve that involves a stochastic nature because the life span has to be closely related to the total metabolic rate spent during the whole life. Despite having the same gene, animals display their individuality or different life history in their aging process. Thus, to get a bird's-eye view of the relation between energy metabolism and survivorship, we superimposed both sets of data, as shown in Fig. 4. According to this figure, the rapid drop of $\dot{V}_{O_2}$ after the fourth day began before the onset of death. This was an unexpected result. It was also very surprising that the respiratory activity of individuals was nearly lost even at an 80% survival rate until 1/2 of the maximum life span had been reached. The declining behavior of respiratory activity appears to correlate with that of the sigmoid curve in survivorship. These results suggest that the process of death coincides with the disappearance of respiratory activity. In the near future, using mutants that have long lives and short lives, we will investigate the present finding in more detail and construct a mathematical model.

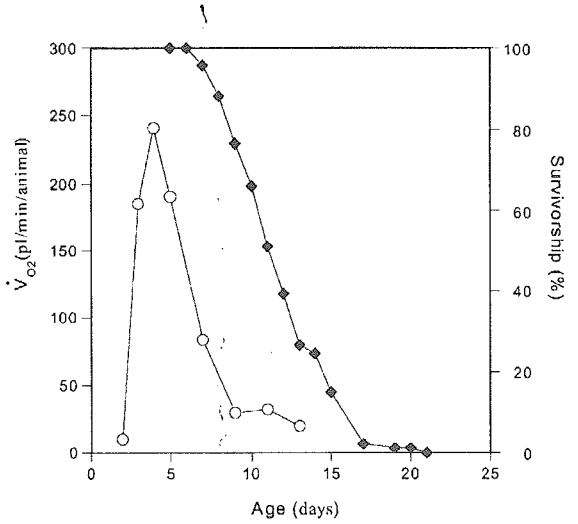

Fig. 4. Oxygen consumption rates and survivorships of wild-type animals at 25 °C. Open circles and filled diamonds represent the $\dot{V}_{O_2}$ per animal and the survivorship, respectively. The $\dot{V}_{O_2}$ data are the same as those shown in Fig. 2A.

Acknowledgments

We thank Drs. Y. Ohshima and M. Fujiwara for the measurement of size of *C. elegans*, and J. Yamamoto for his experimental assistance. The first author dedicates this work to the late O. Suda.

References

[1] L. Guarente, C. Kenyon, Nature 408 (2000) 255–262.
[2] J. Koubova, L. Guarente, Genes Dev. 17 (2003) 313–321.
[3] T. Ozawa, Physiol. Rev. 77 (1997) 425–464.
[4] B.P. Braeckman, K. Houthoofd, A. De Vreese, J.R. Vanfleteren, Aging Cell 1 (2002) 82–88.
[5] K. Houthoofd, B.P. Braeckman, I. Lenaerts, K. Brys, A. De Vreese, S.V. Eygen, J.R. Vanfleteren, Exp. Gerontol. 37 (2002) 1015–1021.
[6] B.P. Braeckman, K. Houthoofd, A. De Vreese, J.R. Vanfleteren, Mech. Ageing Dev. 123 (2002) 105–119.
[7] W.A. Van Voorhies, S. Ward, Proc. Natl. Acad. Sci. USA 96 (1999) 11399–11403.
[8] S. Honda, N. Ishii, K. Suzuki, M. Matsuo, J. Gerontol. 48 (1993) B57–B61.
[9] N. Ishii, M. Fujii, P.S. Hartman, M. Tsuda, K. Yasuda, N. Senoo-Matsuda, S. Yanase, D. Ayusawa, K. Suzuki, Nature 394 (1998) 694–697.
[10] H. Adachi, Y. Fujiwara, N. Ishii, J. Gerontol. 53A (1998) B240–B244.
[11] N. Ishii, K. Takahashi, S. Tomita, T. Keino, S. Honda, K. Yoshino, K. Suzuki, Mutat. Res. 237 (1990) 165–171.
[12] T. Hirose, Y. Nakano, Y. Nagamatsu, T. Misumi, H. Ohta, Y. Ohshima, Development 130 (2003) 1089–1099.
[13] M.R. Klass, Mech. Aging Dev. 6 (1977) 413–429.

Available online at www.sciencedirect.com
SCIENCE DIRECT®
ELSEVIER
Mechanisms of Ageing and Development 126 (2005) 637–641
mechanisms of ageing and development
www.elsevier.com/locate/mechagedev

Effect of oxidative stress on translocation of DAF-16 in oxygen-sensitive mutants, *mev-1* and *gas-1* of *Caenorhabditis elegans*

Masaki Kondo[a,1], Nanami Senoo-Matsuda[a,1], Sumino Yanase[a], Takamasa Ishii[a], Philip S. Hartman[b], Naoaki Ishii[a,*]

[a]*Department of Molecular Life Science, Tokai University School of Medicine, Isehara, Kanagawa 259-1193, Japan*
[b]*Biology Department, Texas Christian University, Fort Worth, TX 76129, USA*

Accepted 11 November 2004
Available online 8 January 2005

Abstract

Mutations in the *mev-1* and *gas-1* genes of the nematode *Caenorhabditis elegans* render animals hypersensitive to oxygen and paraquat, and lead to premature aging. We show that both mutants overproduce superoxide anion in isolated sub-mitochondrial particles, which probably explains their hypersensitivity to oxidative stress. The *daf-16* gene encodes a fork-head transcription factor that is negatively regulated by an insulin-signaling pathway. In wild-type animals, the DAF-16 protein normally resides in the cytoplasm and only becomes translocated to nuclei upon activating stimuli such as oxidative stress. Conversely, DAF-16 resides constitutively in the nuclei of *mev-1* and *gas-1* mutants even under normal growth conditions. Supplementation of the antioxidant coenzyme Q_{10} reversed this nuclear translocation of DAF-16. Since both *gas-1* and *mev-1* encode subunits of electron transport chain complexes, these data illustrate how mitochondrial perturbations can impact signal transduction pathways.

Keywords: Oxidative stress; DAF-16; Mitochondria; *mev-1*; *gas-1*; Coenzyme Q10

1. Introduction

mev-1(*kn1*) and *gas-1*(*fc21*) mutants of the nematode *Caenorhabditis elegans* (*C. elegans*) have several distinct pathophysiologies, including a short life span as well as hypersensitivity to hyperoxia and paraquat (Ishii et al., 1990, 1998; Honda et al., 1993; Senoo-Matsuda et al., 2001; Kayser et al., 1999; Hartman et al., 2001). *mev-1* is defective in a cytochrome b_{560} subunit of complex II and *gas-1* is defective in a Ip (Iron protein) 49 kDa subunit of complex I (Ishii et al., 1998; Kayser et al., 1999). We have demonstrated previously that the *mev-1* phenotypes are caused by overproduction of superoxide anion (O_2^-), a reactive oxygen species (ROS) (Senoo-Matsuda et al., 2001). We now report that the mitochondrial dysfunction of *gas-1* results in overproduction of O_2^- as seen in *mev-1*.

Henderson and Johnson (2001) found that DAF-16 responds rapidly to environmental stressors such as starvation, heat and oxidative stress by moving from the cytoplasm to the nucleus, and subsequently activates transcription. Lifespan in *C. elegans* is regulated in part by an insulin signaling pathway, which signals through the conserved insulin/insulin-like growth factor (IGF)-1 receptor homologue DAF-2 and phosphatidylinositol 3-kinase(PI 3-kinase: *age-1*)/Akt·Sgk pathways (Wolkow et al., 2002; Hertweck et al., 2004). Mutants in this pathway remain youthful and active much longer than normal animals, and they can live more than twice as long. This lifespan extension requires DAF-16, a forkhead/winged-helix tran-

* Corresponding author. Tel.: +81 463 93 1121x2650; fax: +81 463 94 8884.
E-mail address: nishii@is.icc.u-tokai.ac.jp (N. Ishii).
[1] These authors contributed equally to this manuscript.

0047-6374/$ – see front matter © 2004 Elsevier Ireland Ltd. All rights reserved.
doi:10.1016/j.mad.2004.11.011

scription factor. The DAF-16 protein presumably regulates downstream target genes that impact dauer formation, stress resistance, energy metabolism, and life span (Paradis et al., 1999; Lin et al., 1997, 2001; Ogg et al., 1997; Lee et al., 2003; Murphy et al., 2003). The subcellular localization of DAF-16 is regulated by AKT and SGK phosphorylations in the insulin-like signaling pathway (Ogg et al., 1997; Hertweck et al., 2004). DAF-16 is a key regulator of genes that respond to and minimize the effects of oxidative stress (e.g., catalase and superoxide dismutase (SOD)) (Murphy et al., 2003; Honda and Honda, 1999). In this paper, we show that reduction-of-function mutations in *mev-1* and *gas-1* resulted in nuclear localization of DAF-16 even under normal atmospheric conditions. The antioxidant coenzyme Q_{10} (CoQ_{10}), an isoform of coenzyme Q (CoQ) [also known as ubiquinone or 2, 3-dimethoxy-5-methyl-6-multiprenyl-1,4-benzoquinone] (Lass and Sohal, 2000; Kwong et al., 2002) inhibited the translocation of DAF-16 to the nucleus in these mutants. It is likely that the nuclear location of DAF-16 was caused by high steady-state levels of oxidative stress as a consequence of O_2^- overproduction in *gas-1* and *mev-1* mitochondria. Thus, these data indicate that, in addition to exogenous oxidative stress, endogenously created oxidative stress can mediate nuclear localization of DAF-16.

2. Methods

2.1. General methods

C. elegans were cultured as previously described (Brenner, 1974). The wild-type strain (N2) was obtained from the Caenorhabditis Genetics Center (University of Minnesota). CW152 [*gas-1(fc21)* LGX] was kindly provided by P.G. Morgan (Case Western Reserve University). TK22 [*mev-1(kn1)* III] was isolated in this laboratory (Ishii et al., 1990).

2.2. Measurement of O_2^-

For mitochondrial isolation, young adult animals were incubated for 72 h from eggs, harvested by centrifugation and homogenized (10%, w/v) in isolation buffer (210 mM mannitol, 70 mM sucrose, 0.1 mM EDTA and 5 mM Tris–HCl, pH 7.4) with a Teflon homogenizer. Mitochondria were isolated by differential centrifugation (Trounce et al., 1996) and suspended in Tris–EDTA buffer (0.1 mM EDTA, 50 mM Tris–HCl, pH 7.4). Submitochondrial particles (SMP) were obtained by sonicating freeze–thawed mitochondria twice for 20 s separated by 1 min intervals in a model U200S sonicator (IKA Labortechnik). SMP were washed twice and suspended in isolation buffer.

Superoxide anion generation was measured using the chemiluminescent probe MCLA (*cypridina*, luciferin analog, 2-methyl-6-(*p*-methoxyphenol)-3,7-dihydroimidazol [1,2-α] pyrazin-3-one). Forty micrograms of either intact mitochondria or SMP were added to 1 ml of assay buffer (50 mM HEPES, pH 7.4, 2 mM EDTA) containing 0.5 mM MCLA. The solution was placed into the photon counter with a H-R550 photomultiplier (Hamamatsu Photogenic Co. Ltd.) and measured at 37 °C. The rates of superoxide anion production were expressed as counts per second. The amounts were calculated by subtracting the luminescence of MCLA solution including mitochondria from that in MCLA in the absence of the mitochondria.

2.3. Construction of DAF-16::green fluorescent protein (GFP) fusion proteins and transgenics

To construct DAF-16::GFP fusion DNA, a *Sac*II–*Sac*II fragment from a cosmid clone R13H8 was cloned into a plasmid pFXneEGFP vector (kindly obtained from S. Mitani) with a new *Sac*II site in the multi-cloning site. This fragment contains approximately 16.1 kb *daf-16* genomic sequence and approximately 5.9 kb 5′ untranslated region (UTR) of the gene. The constructs were injected into *C. elegans* gonads at 0.05 mg/ml along with 0.1 mg/ml of pRF4 containing *rol-6* (*su1006*).

2.4. Observation with fluorescence microscopy

To create hyperoxia, embryos (eggs) were collected from nematode growth medium (NGM) agar plates using alkaline sodium hypochlorite (Emmons et al., 1979). The released eggs were allowed to hatch by overnight incubation at 20 °C in S basal medium (100 mM NaCl, 50 mM potassium phosphate, pH 6.0) without cholesterol (Sulston and Brenner, 1974). The newly hatched animals were incubated on NGM agar medium until they grew to the second larval (L2) stage. The animals were exposed on NGM agar plates to 90% oxygen for 4 h in an airtight plastic chamber. For CoQ_{10} treatment, L3 larvae were treated on NGM agar including 150 μg/ml CoQ_{10} (C-9538, Sigma, Tokyo) and incubated until progeny L2 larvae appeared on the medium (Ishii et al., 2004). These L2 larvae were observed for the subcellular localization of the GFP fluorescence. We used a microscope with a fluorescence module (Zeiss Axioscope, Carl Zeiss, Tokyo) with a Zeiss exciter band pass filter (Zeiss filter set 09: excitation 450–490 nm), a dichromatic beam splitter FT510 and LP515.

3. Results

3.1. Measurement of O_2^-

Consistent with our previously published data (Senoo-Matsuda et al., 2001), the O_2^- levels were higher in intact mitochondria and SMP from *mev-1* animals than in wild type (Fig. 1). In *gas-1* animals, the levels were higher in the SMP, but unexpectedly, were lower in the intact mitochondria compared to wild type (Fig. 1).

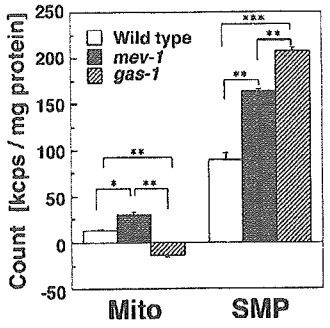

Fig. 1. O_2^- production from mitochondria. Each value reported is the mean ± S.D. of four different experiments. * $P < 0.05$; ** $P < 0.005$; *** $P < 0.001$ by paired Student's test. Mito, intact mitochondria.

3.2. Subcellular localization of DAF-16 in mev-1 and gas-1 mutants under hyperoxia

We constructed a reporter with the green fluorescent protein (GFP) fused to *daf-16* genomic sequences including approximately 5.9 kb of upstream UTR containing a predicted winged-helix DNA binding domain and other upstream regulatory elements (Fig. 2). Most DAF-16 protein was found in the cytoplasm of wild-type animals grown under atmospheric conditions. Conversely, when the animals were subjected to oxidative stress by hyperoxia, DAF16 was translocated to the nucleus (Fig. 3). In contrast, DAF-16 was present in the nucleus of both *mev-1* and *gas-1* mutants, even under atmospheric conditions (Fig. 3). Although L2 larvae were used in these experiments, the result using L4 larvae were the same (unpublished data). The free radical scavenger CoQ_{10} inhibited the translocation of DAF-16 to the nucleus in these mutants (Fig. 3).

4. Discussion

mev-1 (*kn1*) and *gas-1* (*fc21*) mutants of *C. elegans* have several distinct pathophysiologies including a short life span

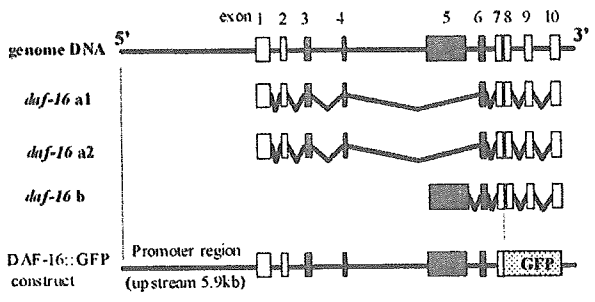

Fig. 2. Structure of the *daf-16* gene, its transcripts, and the DAF-16::GFP construct. Predicted coding regions (open boxes and numbers) including fork head domain coding exon (filled boxes) and introns (lines). DAF-16 a1 and a2 differ by six base pairs as a consequence of alternative 3′ splicing of intron two. The DAF-16::GFP construct includes the genome region from exon one to seven.

and hypersensitivity to oxidative stress in the form of hyperoxia and paraquat (Ishii et al., 1990, 1998; Honda et al., 1993; Senoo-Matsuda et al., 2001; Kayser et al., 1999; Hartman et al., 2001). We have previously established that the levels of oxidative stress are higher in *mev-1* animals; namely, superoxide anion levels are higher in both intact mitochondria and SMP in *mev-1* animals (Senoo-Matsuda et al., 2001). We have both confirmed this relationship (Fig. 1) and have also determined that O_2^- production is significantly higher in SMP from *gas-1* animals (Fig. 1). Surprisingly, O_2^- levels were lower in intact *gas-1* mitochondria compared to wild type (Fig. 1). The difference of O_2^- levels between intact mitochondria and SMP in *gas-1* may be the consequence of Mn-SOD in mitochondria, since SMP isolation could result in Mn-SOD loss. In fact, Mn-SOD was induced in *gas-1* animals such that the mitochondrial level was 1.8-fold greater than wild type (unpublished data). Elevated Mn-SOD levels could act to suppress the steady-state O_2^- levels in intact *gas-1* mitochondria, even though more O_2^- is generated. Mn-SOD induction in response to oxidative stress has been previously reported. For example, Esposito et al., 1999 observed substantial increases in Mn-SOD in the muscle and heart of *Ant* mutant mice. These animals possess a mitochondrial defect that results in elevated oxidative stress. It is possible that the most damaging ROS in *gas-1* mitochondria may be hydrogen peroxide or hydroxyl radicals caused by the action of Mn-SOD on O_2^-. Recently, we found that mutation frequencies in the nucleus are elevated in *mev-1* (Hartman et al., 2004) but not in *gas-1* (Hartman et al., 2001) animals. The difference in persistence of O_2^- in *gas-1* versus *mev-1* may explain this.

Henderson and Johnson (2001) found that DAF-16 responds rapidly to environmental stressors such as starvation, heat and oxidative stress by moving from the cytoplasm to the nucleus, and thus activates transcription. Much attention has focused on the insulin-like signaling pathway in *C. elegans* because of its pivotal role in life-span determination and oxidative stress resistance (Paradis et al., 1999; Lin et al., 1997, 2001; Ogg et al., 1997; Lee et al., 2003; Murphy et al., 2003). The *daf-16* gene plays a pivotal role in this pathway and encodes a fork-head transcription factor that is negatively regulated by upstream elements. Activated by dephosphorylation, DAF-16 is translocated from its normal cytoplasmic location to the nucleus, where it regulates downstream target genes that impact dauer formation, stress resistance, energy metabolism and life span. We constructed a reporter with GFP fused to *daf-16* genomic sequences including approximately 5.9 kb of upstream UTR containing a predicted winged-helix DNA binding domain and other upstream regulatory elements (Fig. 2). The *daf-16* gene normally produces three different transcripts: a1, a2 and b (Lin et al., 1997; Ogg et al., 1997). Consistent with a published report by Henderson and Johnson (2001), we found most DAF-16 protein to be located in the cytoplasm of wild-type animals exposed to

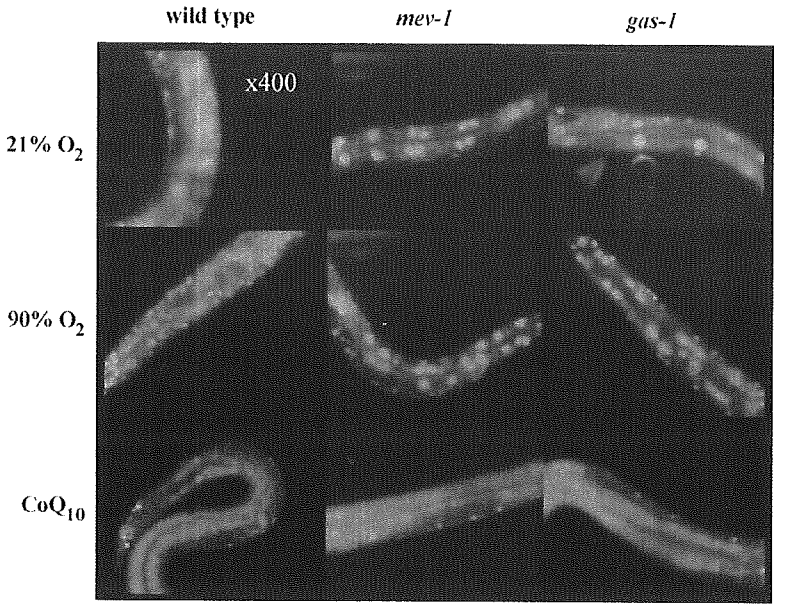

Fig. 3. Localization of DAF-16::GFP in wild type, *mev-1* and *gas-1* L2 larvae under atmospheric conditions (21% oxygen), 90% oxygen and CoQ_{10}.

low levels of oxidative stress (Fig. 3). On the other hand, DAF-16 was present in the nuclei of *mev-1* and *gas-1* mutants, even under the normal atmospheric conditions (Fig. 3). We have reported previously that the antioxidant CoQ_{10} reduces O_2^- levels in the *mev-1* mutant (Ishii et al., 2004). As shown in Fig. 3, the antioxidant CoQ_{10} perfectly inhibited the translocation of DAF-16 to the nucleus in both *mev-1* and *gas-1* animals. It is true that CoQ plays a number of additional roles in living organisms, including in respiration itself. However, two factors cause us to favor the explanation that, at least in these experiments, CoQ_{10} acts as an antioxidant. First, both *mev-1* and *gas-1* are wild type with respect to CoQ_9 synthesis and therefore there is no reason to believe the respiratory defects in these two mutants are directly related to CoQ_{10} levels. Second, we employed relatively high levels of CoQ_{10} in these experiments, such that ROS scavenging should be maximal. While ROS levels were elevated in *gas-1* sub-mitochondrial particles, they were not in intact *gas-1* mitochondria. This suggests that the *gas-1* mutant produces excess superoxide anion, but steady-state levels in intact mitochondria are relatively low owing to the action of Mn-SOD. However, we hypothesize that superoxide anion leaks from *gas-1* mitochondria to create cytoplasmic oxidative stress, leading to DAF-16 translocation in *gas-1* animals. Without such an explanation, it is difficult to reconcile the fact that superoxide anion levels are low in *gas-1* mitochondria with the observation that DAF-16 is localized to nuclei in both *mev-1* and *gas-1* mutants.

Henderson and Johnson (2001) showed that DAF-16 is translocated from the cytoplasm to the nucleus in wild-type animals when exposed to exogenous oxidative stress. This nuclear translocation activates a number of downstream events that promote stress resistance and longevity (Murphy et al., 2003; Lee et al., 2003). These observations lead to the prediction that *mev-1* and *gas-1* should be resistant rather than sensitive to oxidative stress, as we have previously documented (Hartman et al., 2001). Indeed, Mn-SOD is overexpressed in *gas-1* (data not shown). However, we speculate that these two mutants are hypersensitive to oxidative stress because their mitochondria overproduce ROS (Fig. 1), which overwhelms any and all resistance mechanisms afforded by DAF-16 translocation.

Finally, we note that ROS are continuously produced in living organs as byproducts of normal energy metabolism. Our data suggest that such endogenously generated molecules cannot only readily attack a wide variety of cellular entities, but also trigger signaling pathways that lead to transcriptional activation of downstream targets in a pathway.

Acknowledgement

This work is funded in part by grants of the Virtual Research Institute of Aging of Nippon Boehringer Ingelheim.

References

Brenner, S., 1974. The genetics of *Caenorhabditis elegans*. Genetics 77, 71–94.

Emmons, S.W., Klass, M.R., Hirsh, D., 1979. Analysis of the constancy of DNA sequences during development and evolution of the nematode *Caenorhabditis elegans*. Proc. Natl. Acad. Sci. U.S.A. 76, 1333–1337.

Esposito, L.A., Melov, S., Panov, A., Cottrell, B.A., Wallace, D.C., 1999. Mitochondrial disease in mouse results in increased oxidative stress. Proc. Natl. Acad. Sci. U.S.A. 96, 4820–4825.

Hartman, P.S., Ishii, N., Kayser, E.-B., Morgan, P.G., Sedensky, M.M., 2001. Mitochondrial mutations differentially affect aging, mutability and anesthetic sensitivity in *Caenorhabditis elegans*. Mech. Ageing Dev. 122, 1187–1201.

Hartman, P., Ponder, R., Lo, H.H., Ishii, N., 2004. Mitochondrial oxidative stress can lead to nuclear hypermutability. Mech. Ageing Dev. 125, 417–420.

Henderson, S.T., Johnson, T.E., 2001. *daf-16* integrates developmental and environmental inputs to mediate aging in the nematode *Caenorhabditis elegans*. Curr. Biol. 11, 1975–1980.

Hertweck, M., Gobel, C., Baumeister, R., 2004. *C. elegans* SGK-1 is the critical component in the Akt/PKB kinase complex to control stress response and life span. Dev. Cell 6, 577–588.

Honda, S., Ishii, N., Suzuki, K., Matsuo, M., 1993. Oxygen-dependent perturbation of life span and aging rate in the nematode. J. Gerontol. 48, B57–B61.

Honda, Y., Honda, S., 1999. The *daf-2* gene network for longevity regulates oxidative stress resistance and Mn-superoxide dismutase gene expression in *Caenorhabditis elegans*. FASEB J. 13, 1385–1393.

Ishii, N., Takahashi, K., Tomita, S., Keino, T., Honda, S., Yoshino, K., Suzuki, K., 1990. A methyl viologen-sensitive mutant of the nematode *Caenorhabditis elegans*. Mutat. Res. 237, 165–171.

Ishii, N., Fujii, M., Hartman, P.S., Tsuda, M., Yasuda, K., Senoo-Matsuda, N., Yanase, S., Ayusawa, D., Suzuki, K., 1998. A mutation in succinate dehydrogenase cytochrome *b* causes oxidative stress and ageing in nematodes. Nature 394, 694–697.

Ishii, N., Senoo-Matsuda, N., Miyake, K., Yasuda, K., Ishii, T., Hartman, P.S., Furukawa, S., 2004. Coenzyme Q_{10} can prolong *C. elegans* lifespan by lowering oxidative stress. Mech. Ageing Dev. 125, 41–46.

Kayser, E.-B., Morgan, P.G., Sedensky, M.M., 1999. GAS-1: a mitochondrial protein controls sensitivity to volatile anesthetics in the nematode *Caenorhabditis elegans*. Anesthesiology 90, 545–554.

Kwong, L.K., Kamzalov, S., Rebrin, I., Bayne, A.-C.V., Jana, C.K., Morris, P., Forster, M.J., Sohal, R.S., 2002. Effects of coenzyme Q_{10} administration on its tissue concentrations, mitochondrial oxidant generation, and oxidative stress in the rat. Free Radic. Biol. Med. 33, 627–638.

Lass, A., Sohal, R.S., 2000. Effect of coenzyme Q_{10} and α-tocopherol content of mitochondria on the production of superoxide anion radicals. FASEB J. 14, 87–94.

Lee, S.S., Kennedy, S., Tolonen, A.C., Ruvkun, G., 2003. DAF-16 target genes that control *C. elegans* life-span and metabolism. Science 300, 644–647.

Lin, K., Dorman, J.B., Rodan, A., Kenyon, C., 1997. *daf-16*: An HNF-3/forkhead family member that can function to double the life-span of *Caenorhabditis elegans*. Science 278, 1319–1322.

Lin, K., Hsin, H., Libina, N., Kenyon, C., 2001. Regulation of the *Caenorhabditis elegans* longevity protein DAF-16 by insulin/IGF-1 and germline signaling. Nat. Genet. 28, 139–145.

Murphy, C.T., McCarroll, S.A., Bargmann, C.I., Fraser, A., Kamath, R.S., Ahringer, J., Li, H., Kenyon, C., 2003. Genes that act downstream of DAF-16 to influence the lifespan of *Caenorhabditis elegans*. Nature 424, 277–284.

Ogg, S., Paradis, S., Gottlieb, S., Patterson, G.I., Lee, L., Tissenbaum, H.A., Ruvkun, G., 1997. The fork head transcription factor DAF-16 transduces insulin-like metabolic and longevity signals in *C. elegans*. Nature 389, 994–999.

Paradis, S., Ailion, M., Toker, A., Thomas, J.H., Ruvkun, G., 1999. A PDK1 homolog is necessary and sufficient to transduce AGE-1 PI3 kinase signals that regulate diapause in *Caenorhabditis elegans*. Genes Dev. 13, 1438–1452.

Senoo-Matsuda, N., Yasuda, K., Tsuda, M., Ohkubo, T., Yoshimura, S., Nakazawa, H., Hartman, P.S., Ishii, N., 2001. A defect in the cytochrome *b* large subunit in complex II causes both superoxide anion overproduction and abnormal energy metabolism in *Caenorhabditis elegans*. J. Biol. Chem. 276, 41553–41558.

Sulston, J.E., Brenner, S., 1974. The DNA of *Caenorhabditis elegans*. Genetics 77, 95–104.

Trounce, I.A., Kim, Y.L., Jun, A.S., Wallace, D.C., 1996. Assessment of mitochondrial oxidative phosphorylation in patient muscle biopsies, lymphoblasts, and transmitochondrial cell lines. Meth. Enzymol. 264, 484–509.

Wolkow, C.A., Munoz, M.J., Riddle, D.L., Ruvkun, G., 2002. Insulin receptor substrate and p55 orthologous adaptor proteins function in the *Caenorhabditis elegans daf-2*/insulin-like signaling pathway. J. Biol. Chem. 277, 49591–49597.

Available online at www.sciencedirect.com
SCIENCE DIRECT®
ELSEVIER
Mechanisms of Ageing and Development 126 (2005) 642–647
mechanisms of ageing and development
www.elsevier.com/locate/mechagedev

The p38 signal transduction pathway participates in the oxidative stress-mediated translocation of DAF-16 to *Caenorhabditis elegans* nuclei

Masaki Kondo[a,1], Sumino Yanase[a,1], Takamasa Ishii[a], Philip S. Hartman[b], Kunihiro Matsumoto[c], Naoaki Ishii[a,*]

[a]*Department of Molecular Life Science, Tokai University School of Medicine, Isehara, Kanagawa 259-1193, Japan*
[b]*Biology Department, Texas Christian University, Fort Worth, TX 76129, USA*
[c]*Department of Molecular Biology, Graduate School of Science, Nagoya University, Chikusa-ku, Nagoya 464-8602, Japan*

Accepted 11 November 2004
Available online 11 January 2005

Abstract

Much attention has focused on the insulin-like signaling pathway in *Caenorhabditis elegans* because of its pivotal role in life-span determination and oxidative stress resistance. The *daf-16* gene encodes a fork-head transcription factor that is negatively regulated by this insulin-signaling pathway. The DAF-16 protein is translocated to the nucleus when animals were subjected to oxidative stress in the form of paraquat. This oxidative stress-mediated translocation was blocked by mutation of the p38-related *sek-1* (MAPKK) mutant and DAF-16 instead remained cytoplasmic. The fact that DAF-16 translocation by oxidative stress is epistatic to *sek-1* suggests that oxidative stress mediates regulation of DAF-16 through activating the p38 signal transduction pathway upstream of *daf-16* so as to mobilize DAF-16 to the nucleus and activate transcription.

Keywords: Oxidative stress; p38 signal transduction pathway; DAF-16; *C. elegans*; *sek-1*

1. Introduction

The *Caenorhabditis elegans* insulin-like signaling pathway operates through a conserved insulin/insulin-like growth factor (IGF)-1 receptor homolog DAF-2 and controls the cellular location of DAF-16. The *daf-16* gene encodes a FOXO class forkhead/winged-helix transcription factor that is negatively regulated by the insulin-signaling pathway. The DAF-16 protein presumably regulates downstream target genes that impact dauer formation, stress resistance, energy metabolism and life span (Paradis et al., 1999; Lin et al., 1997, 2001; Ogg et al., 1997; Murphy et al., 2003). The subcellular localization of DAF-16 is regulated by AKT and SGK phosphorylations (Ogg et al., 1997; Hertweck et al., 2004). It is speculated that AKT phosphorylation generates 14-3-3 binding sites and regulates the translocation of DAF-16. A 14-3-3-independent pathway may also mediate DAF-16 translocation (Cahill et al., 2001). DAF-16 is a key regulator of genes that respond to and minimize the effects of oxidative stress (e.g., catalase and superoxide dismutase) (Murphy et al., 2003; Honda and Honda, 1999). DAF-16 responds rapidly to environmental stressors such as starvation, heat and oxidative stress by moving from the cytoplasm to the nucleus (Henderson and Johnson, 2001) thus presumably activating transcription. DAF-16 is thought to be the main target of the DAF-2 pathway, because the activity of *daf-16* is required for all Daf-2(–) phenotypes. Moreover, several large-scale mutagenesis screens showed that all zygotic *daf-2* suppressor mutations were in *daf-16* mutations (Lin et al., 1997). Despite this evidence, we questioned whether reactive oxygen species (ROS) directly

* Corresponding author. Tel.: +81 463 93 1121x2650; fax: +81 463 94 8884.
E-mail address: nishii@is.icc.u-tokai.ac.jp (N. Ishii).
[1] These authors contributed equally to this manuscript.

0047-6374/$ – see front matter © 2004 Elsevier Ireland Ltd. All rights reserved.
doi:10.1016/j.mad.2004.11.012

activate the DAF-2 signal pathway. Therefore, we examined signaling pathways that are known to respond to ROS signals in other organisms to see if they play a role in the activation of DAF-16 in *C. elegans*. In this report, we show that oxidative stress-mediated translocation was blocked by mutation of the p38-related *sek-1* (MAPKK) mutant and DAF-16 instead remained cytoplasmic. *sek-1* mutants were found to be hypersensitive to oxidative stress produced by paraquat. The fact that DAF-16 translocation by oxidative stress is epistatic to *sek-1* suggests that oxidative stress mediates regulation of DAF-16 through activating the p38 signal transduction pathway upstream of *daf-16* so as to mobilize DAF-16 to the nucleus and activate transcription.

2. Methods

2.1. General methods

C. elegans were cultured as previous described (Brenner, 1974). Mutants used in this study were: *daf-16(m26)* LGI, *jnk-1(gk7)* LGIV, *mek-1(ks54)* LGX, *sek-1(km4)* LGX, *nsy-1(ky397)* LGII. The wild-type strain, *daf-16*, *jnk-1* and *mek-1* mutants were obtained from the Caenorhabditis Genetics Center.

2.2. Construction of DAF-16::green fluorescent protein (GFP) fusion proteins and transgenics

The *daf-16* gene normally produces three different transcripts: a1, a2 and b (Fig. 1). To construct DAF-16::GFP fusion DNA, a *Sac*II–*Sac*II fragment from a cosmid clone R13H8 was cloned into a plasmid pFXneEGFP vector (kindly obtained from S. Mitani) with a new *Sac*II site in the multi-cloning site. This fragment contains approximately 16.1 kb *daf-16* genomic sequence and approximately 5.9 kb 5′ untranslated region (UTR) containing a predicted winged-helix DNA binding domain and other upstream regulatory elements (Fig. 1). The construct was injected into *C. elegans* gonads at 0.05 mg/ml with 0.1 mg/ml of pRF4 containing *rol-6* (*su1006*).

2.3. Observation with fluorescence microscopy

Embryos (eggs) were collected from nematode growth medium (NGM) agar plates using alkaline sodium hypochlorite (Emmons et al., 1979). The released eggs were allowed to hatch by overnight incubation at 20 °C in S basal medium (100 mM NaCl, 50 mM potassium phosphate (pH 6.0) (Sulston and Brenner, 1974) without cholesterol. The newly hatched larvae were incubated NGM agar medium until they reached the second larval stage (L2's). The animals were treated with 0.3 mM paraquat for 4 h in S basal medium without cholesterol before observations. The animals were then observed for the subcellular localization of GFP fluorescence. We used a microscope with a fluorescence module (Zeiss Axioscope, Carl Zeiss, Tokyo) with a Zeiss exciter band pass filter (Zeiss filter set 09: excitation 450–490 nm), a dichromatic beam splitter FT510 and LP515.

2.4. Paraquat sensiivity

L1 larvae were cultured on seeded nematode growth (NGM) agar plates containing various concentration of

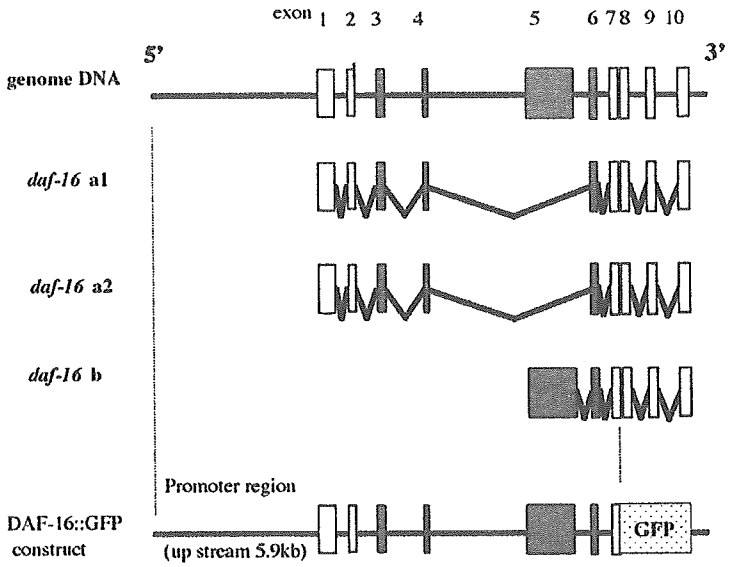

Fig. 1. Structure of the *daf-16* gene, its transcripts and the DAF-16::GFP construct. Predicted coding regions (open boxes and numbers) including fork head domain coding exon (filled boxes) and introns (lines). DAF-16 a1 and a2 differ by six base pairs as a consequence of alternative 3′ splicing of intron two. The DAF-16::GFP construct includes the genome region from exon one to seven.

paraquat. Four days later, survival was determined by counting the number of L4 larvae and adults.

3. Results

3.1. Subcellular localization of DAF-16

In eukaryotic cells, the mitogen-activated protein kinases (MAPKs) transduce signals in response to a variety of extracellular stimuli. MAPKs are classified into three subfamilies: the extracelluar signal-regulated kinase (ERKs), c-Jun N-terminal kinase (JNK) and p38 (Fig. 2A) (Kyriakis and Avruch, 1996; Robinson and Cobb, 1997; Ip and Davis, 1998). JNK and p38 are primed to respond to stress by virtue of a stress-activated protein kinase and a cytokine-suppressive anti-inflammatory drug-binding protein kinase, respectively. In *C. elegans*, the JNK pathway has been shown to function in both synapse vesicle transport and heavy metal resistance; and p38 plays a role in the generation of neuronal asymmetry by Ca^{2+} signaling as well as in immune responses (Fig. 2B) (Byrd et al., 2001; Koga et al., 2000; Villanueva et al., 2001; Tanaka-Hino et al., 2002; Kim et al., 2002).

Most DAF-16 protein was found in the cytoplasm of wild-type animals grown under low levels of oxidative stress (Fig. 3). Similar results were observed in three mutants [*jnk-1* (JNK-related MAPK), *mek-1* (JNK-related MAPKK) and *sek-1* (p38-related MAPKK)], each of which is defective in one predicted signaling pathway (Fig. 3). Conversely, DAF-16 was also found in the nuclei of wild-type animals as well as *jnk-1* and *mek-1* mutants when they were subjected to oxidative stress in the form of paraquat (Fig. 3). In the *sek-1* mutant, however, DAF-16 remained primarily in the cytoplasm even in the face of oxidative stress (Fig. 3).

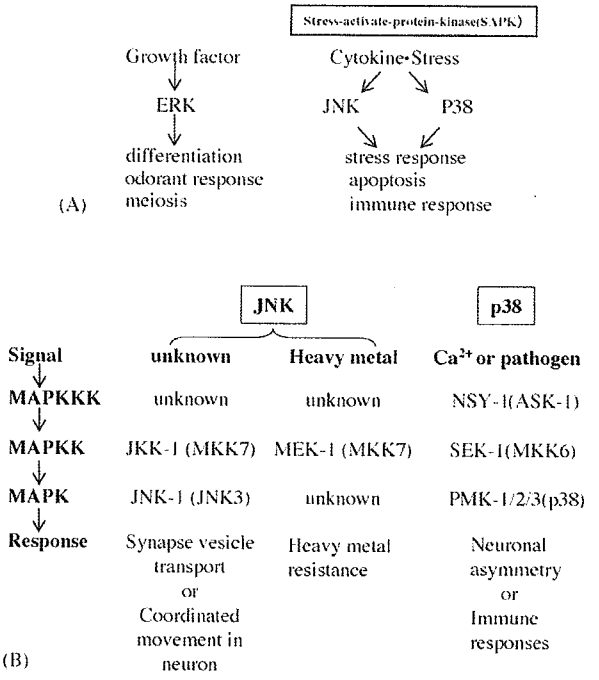

Fig. 2. (A) Overview of generic MAP kinase signal transduction pathways. (B) Predicted MAP kinase (JNK and p38) pathways in *C. elegans*.

3.2. Paraquat sensitivities

Both the p38-related *nsy-1* (MAPKKK) and *sek-1* (MAPKK) mutants are hypersensitive to oxidative stress as presented by paraquat (Fig. 4A). Conversely, *daf-16* was only slightly hypersensitive, suggesting that the p38 pathway regulates resistance to ROS by downstream elements in addition to *daf-16*. This is consistent with fact that the *sek-1*; *daf-16* double mutant showed the same degree of hypersensitivity as the *sek-1* single mutant (Fig. 4A). In

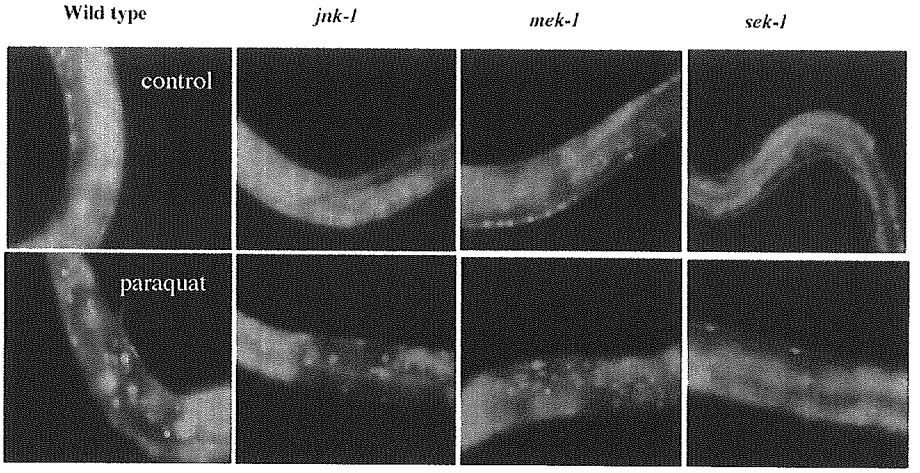

Fig. 3. Localization of DAF-16::GFP in wild-type animals, *jnk-1* (MAPK in the JNK pathway), *mek-1* (MAPKK in the JNK pathway) and *sek-1* (MAPKK is the p38 pathway) mutants.